

Article

Synthesis of a 5-Carboxy Indole-Based Spiropyran Fluorophore: Thermal, Electrochemical, Photophysical and Bovine Serum Albumin Interaction Investigations

Rodrigo da Costa Duarte ¹, Fabiano da Silveira Santos ¹, Bruno Bercini de Araújo ², Rodrigo Cercena ¹ , Daniela Brondani ³ , Eduardo Zapp ³, Paulo Fernando Bruno Gonçalves ² , Fabiano Severo Rodembusch ^{2,*}  and Alexandre Gonçalves Dal-Bó ^{1,*} 

¹ Programa de Pós-Graduação em Ciência e Engenharia de Materiais–PPGCEM, Universidade do Extremo Sul Catarinense (UNESC), Criciúma CEP 88806-000, Brazil; duarte.rodrigo01@gmail.com (R.d.C.D.); fabianofss@gmail.com (F.d.S.S.); rcercena@gmail.com (R.C.)

² Instituto de Química, Universidade Federal do Rio Grande do Sul (UFRGS), Porto Alegre CEP 91501-970, Brazil; bruno.bercini@gmail.com (B.B.d.A.); paulo@iq.ufrgs.br (P.F.B.G.)

³ Departamento de Ciências Exatas e Educação (CEE), Universidade Federal de Santa Catarina (UFSC), Blumenau 89036-004, Brazil; daniela.brondani@ufsc.br (D.B.); eduardo.zapp@ufsc.br (E.Z.)

* Correspondence: rodembusch@iq.ufrgs.br (F.S.R.); adalbo@unesc.net (A.G.D.-B.)

Received: 3 April 2020; Accepted: 27 April 2020; Published: 3 May 2020

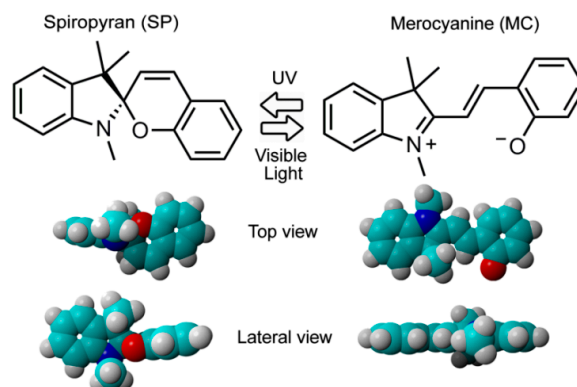


Abstract: In this study, we synthesized a spiropyran containing an electron-withdrawing carboxyl group in good yield by condensation of an aromatic aldehyde with enamine indole. The spiropyran absorbed at the ultraviolet region with a maximum at approximately 300 nm, demonstrating slight solvatochromism (~3 nm). A fluorescent emission around 360 nm was observed with a higher solvatochromic effect (~12 nm), indicating higher electronic delocalization in the excited state. The photoreversibility of the open and closed forms of spiropyran excited at 300 nm and 365 nm was not observed, indicating that the absence of the nitro group plays a fundamental role in this equilibrium. Theoretical calculations were also applied for better understanding the photophysics of these compounds. Electrochemical characterization revealed the values of the HOMO and LUMO energy levels at -1.89 eV (electron affinity) and -5.61 eV (ionization potential), respectively. Thermogravimetric analysis showed excellent thermal stability of the spiropyran, with 5% weight loss at approximately 250 °C. Finally, the photophysical features were used to explore the interaction of spiropyran with bovine serum albumin in a phosphate buffer solution, where a significant suppression mechanism was observed.

Keywords: spiropyran; fluorescence; quenching; optical sensor; Stern–Volmer

1. Introduction

Spiroyrans are a class of organic molecules widely studied for their photochromic properties [1,2]. Their relatively easy structural modification allows for control of their photodynamic characteristics in different media [3–7]. The considerable difference in the physicochemical properties of spiropyran between the initial and the photoinduced form is also of interest [8–12]. These molecules may undergo heterolytic C–O bond cleavage in the spiro form, resulting in an open zwitterionic form, merocyanine (Scheme 1) [13].



Scheme 1. Basic equilibrium between the spiropyran and merocyanine species of a non-substituted spiropyran.

The orthogonal spiro form does not absorb visible light, and it is converted to the planar and colored merocyanine form by excitation under ultraviolet light. The structural transformation of spiropyran to merocyanine is accompanied by increased polarity, and the initial form is regenerated by absorption in the visual or thermal region [14–17]. These molecules demonstrate various phenomena, such as photochromism [18,19], solvatochromism [20,21], thermochromism [22], hydrochromism [23], and acidochromism [24], when stimulated by light, solvents, heat, water, and acid/base, respectively [25]. In addition, spiropyran compounds may exhibit solvatochromism at different solvent polarities. The highly polar form of merocyanine can lead to hypsochromic or bathochromic changes depending on the solvent polarity. Thus, spiropyrans can be used as indicators of solvent polarity owing to their negative solvatochromism [26,27]. Reversible transformation of spiropyrans has been widely used in many areas, including fluorescence modulation of nanoparticles [28,29], amino acid recognition and quantification [30], optical devices [31], proton transfer induction [32], photosensitive biomaterials [33], and pH and ion sensors [24,34]. The interaction between the spiropyran and the merocyanine form is viable because of the oxygen atom. However, the additional binding site leads to the much more stable merocyanine form and aids in the detection of metal ions. Thus, spiropyran and its derivatives have been utilized for the quantitative and qualitative detection of various metal ions [7,35,36].

Herein, we present the synthesis of a spiropyran derivative, its thermal, electrochemical, and photophysical characterization, and its application as a fluorescent probe to detect proteins in a phosphate buffer solution (PBS) using bovine serum albumin (BSA) as a protein model.

2. Materials and Methods

The compounds *p*-Aminobenzoic acid, salicylaldehyde, 3-methyl-2-butanone, ammonium acetate, and $\text{SnCl}_2 \cdot 2\text{H}_2\text{O}$ were purchased from Sigma-Aldrich. NaNO_2 , HCl, MeOH, and CH_3COOH were acquired from Synth. The reagents and solvents were used as received or purified according to the literature using standard procedures [37]. The chemical reactions were monitored by thin layer chromatography using Silica Gel 60 F254 plates. Purification of the compounds was performed by column chromatography using 70–230 mesh Silica Gel 60 Å. Infrared spectra (4000 to 750 cm^{-1}) were acquired using NaCl disk in a Shimadzu-IR PRESTIGE-21 spectrometer with 4.0 resolution and 20 scans. ^1H and ^{13}C NMR spectra were obtained with a Bruker Scientific operating at 400 MHz (^1H) or 100 MHz (^{13}C) using deuterated chloroform (CDCl_3). The chemical shifts (δ) were measured in ppm, and the coupling constants (J) in Hz. ^1H NMR spectra were presented regarding their multiplicities (s, singlet; d, doublet; m, multiplet), integrals and coupling constants.

The compound 1',3'-Dihydro-1',3',3'-trimethylspiro[2*H*-1-benzopyran-2,2'-(2*H*)-indole]-5'-carboxylic acid, so-called Spiropyran 7 was synthesized by the addition of 5-carboxy-1,2,3,3-tetramethyl-3*H*-indol-1-ium iodide 5 (172 mg, 0.49 mmol) in 20 mL of methanol, followed by the addition of $\text{CH}_3\text{COONH}_4$ (77 mg, 1.0 mmol). This mixture was stirred for 5 min at 25 °C. Then compound 6 (61 mg, 0.5 mmol) was added to the reaction mixture under stirring and reflux for 24 h. After the

solvent was evaporated under vacuum, the solid was purified by precipitation and washed with hexane (6 × 50 mL).

1',3'-Dihydro-1',3',3'-trimethylspiro[2H-1-benzopyran-2,2'-(2H)-indole]-5'-carboxylic acid. Brown solid, yield 51%, melting point: 256–259 °C. FTIR (NaCl) ν_{\max} (cm⁻¹): 2967, 2807, 1660, 1609, 1297, 1246. ¹H NMR (CDCl₃, 400 MHz): δ (ppm) 8.06 (d, 1H, *J* = 8 Hz); 7.83 (s, 1H); 7.12 (m, 2H); 6.92 (d, 1H, *J* = 10.27 Hz); 6.88 (m, 1H); 6.74 (d, 1H, *J* = 8.31 Hz); 6.56 (d, 1H, *J* = 8.31 Hz); 5.70 (d, 1H, *J* = 10.27 Hz); 2.85 (s, 3H); 1.38 (s, 3H); 1.21 (s, 3H). ¹³C NMR (CDCl₃, 100 MHz) δ (ppm) 172.4; 154.0; 152.8; 136.8; 132.5; 129.9; 129.8; 126.8; 123.8; 120.4; 119.6; 118.5; 118.4; 115.0; 105.8; 104.1; 51.3; 28.7; 25.8; 20.1.

UV-Vis absorption spectra in solution (10⁻⁵ M) were obtained with a Shimadzu UV-2450 spectrophotometer. Steady-state fluorescence emission spectra were acquired using a Shimadzu RF-5301PC spectrofluorometer. The maximum absorption was used as the excitation wavelength for emission spectra. Slits of 5.0 nm/5.0 nm were used for emission/excitation, respectively. The quantum yield of fluorescence was measured at 25 °C using quinine sulfate (1 N H₂SO₄) as the quantum yield standard [38] at the optical dilute regime (absorbance lower than 0.1).

Photoisomerization experiments were conducted in solution using acetonitrile as the solvent (~10⁻⁵ M). The absorption spectra were acquired in two different ways: (i) one spectrum every 2 min for 50 min and (ii) one after 5 min of irradiation at 300 nm and 365 nm on a Hewlett-Packard 8452A diode array spectrophotometer-registered using a homemade LabView® interface. An Hg/Xe 200-W lamp from ThermoOriel was assembled perpendicularly to the spectrophotometer to induce photoisomerization.

Cyclic voltammetry (CV) was performed on a PalmSens3 potentiostat/galvanostat, using a solution of tetra-*N*-butylammonium hexafluorophosphate (TBAPF₆) in CH₂Cl₂ (0.1 M) as the supporting electrolyte. A three-electrode cell was used, comprised of a glassy carbon electrode as the working electrode, a platinum wire as the counter electrode, and an Ag/Ag⁺ reference electrode. The cell was deoxygenated by purging with argon before each measurement. Ferrocene/ferricenium (Fc/Fc⁺) redox couple was used as internal reference.

Thermogravimetric analysis (TGA) and differential scanning calorimetry (DSC) were also used to better characterize the thermal behavior of the synthesized compound. DSC was carried out on a DSC Sirius from Netzsch under nitrogen atmosphere at a heating rate of 10 °C·min⁻¹. The melting point (*T*_m) and glass transition temperature (*T*_g) were taken from the first and second heating curves, respectively. TGA was carried out on a Shimadzu TG-50 analyzer under nitrogen atmosphere at a heating rate of 10 °C·min⁻¹ (25 °C–1000 °C). The mass of the samples was between 3 and 7 mg.

The ionization constant (*pK*_a) was obtained according to the literature [39]. The proton concentration was measured with a Digimed DM-22 pH-meter with flow-through glass-silver chloride electrodes filled with a saturated solution of potassium chloride. The titrations in solution were performed with a constant ionic strength (μ = 0.1) by the addition of 0.15 M KCl [40]. UV-Vis spectra were performed in an EtOH/H₂O solution (1:1 *v/v*) at different pH using a Shimadzu UV-2450 spectrophotometer [41,42]. In the data treatment, the sum of squared residuals of absorbance intensity values as a function of wavelength under different pH conditions was minimized with a Boltzmann sigmoidal regression function. The pH vs. absorbance data were adjusted with good correlation coefficients. The inflection point indicated the equivalence of pH to *pK*_a according to the Henderson–Hasselbach equation [43].

The bovine serum albumin (BSA) suppression study was performed by keeping the protein concentration constant (7.33 × 10⁻⁶ M in PBS buffer, pH 7.2) during addition of previously prepared spiropyran solutions in dimethylformamide (0–20.5 μM). The final solution was left to rest for 1 h. The fluorescence spectra were obtained under excitation at 279 nm at 25 °C, using emission/excitation slits of 5.0 nm/5.0 nm, respectively. The bovine serum albumin (BSA) association study was performed by keeping the spiropyran concentration constant (1.86 μM in dimethylformamide) during the addition of a previously prepared BSA solutions in PBS buffer (0–8.0 μM, pH 7.2). The final solution was

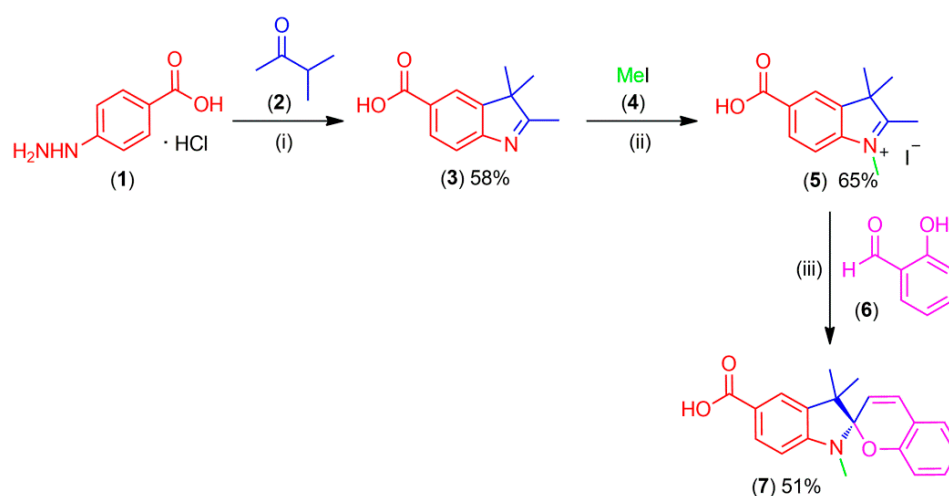
left to rest for 1 h. The fluorescence spectra were obtained under excitation at 298 nm at 25 °C, using emission/excitation slits of 5.0 nm/5.0 nm, respectively.

The theoretical calculations were carried out with density functional theory (DFT) and time dependent density functional theory (TD-DFT) implemented in Gaussian 16 package [44]. The equilibrium geometries in ground and excited states, characterized by the absence of imaginary frequencies, were obtained at PBE1PBE/cc-pVDZ level of theory. The vertical excitation energies were computed for the first ten excited states at PBE1PBE/jun-cc-pVTZ level of theory. PBE1PBE [45] functional was chosen because of the good agreement between the theoretical and experimental results. The jun-cc-pVTZ basis set was chosen for the necessity of diffuse functions to describe the excited states [46]. To simulate the solvent effects, a polarizable continuum model (PCM) was used [47]. To evaluate charge transfer character in spiropyran, Multiwfn package was employed to analyze the increment and depletion zones of electronic densities [48,49]. All the geometries, orbitals, and increment and depletion regions images were rendered with ChemCraft [50].

3. Results and Discussion

3.1. Synthesis of Spiropyran

The heterocycle compound **3** was prepared according to the literature (Scheme 2) [36]. Initially, 4-hydrazinobenzoic acid **1** reacted with 3-methylbutan-2-one **2** under reflux to obtain the intermediate compound 2,3,3-trimethyl-3*H*-indole-5-carboxylic acid **3** by Fischer cyclization [51]. Then, **3** was alkylated with iodomethane **4** in a nitrogen atmosphere to obtain compound **5** [52]. The spectroscopic characterization of compounds **3** and **5**, as well as their synthetic details are presented as supplementary material. The desired spiropyran **7** was synthesized by the reaction of the previously prepared compound **5** with salicylaldehyde **6** under reflux in the presence of ammonium acetate and bases, as required for the Knoevenagel condensation [1]. Spectroscopic characterization indicated that the synthesized spiropyran **7** had a closed structure. The original spectra can be found in the supplementary material (Figures S1–S7). The ¹H NMR spectra indicated the typical signals located at 5.70 (doublet, 1H) and 6.92 (doublet, 1H) with a coupling constant of 10.27 Hz, related to the *cis* conformation, for both vinyl hydrogen atoms. In addition, the O–H stretch in the Fourier-transform infrared (FTIR) spectra appeared as a very broad band at 3300–2500 cm⁻¹, centered at about 3000 cm⁻¹, indicating that compound **7** was present in its acidic form. Furthermore, the UV-Vis spectra exhibited absorption at 300 nm in acidic pH, which corroborated the acidic form indications of the FTIR spectra.



Scheme 2. Synthesis of spiropyran **7**, where (i) CH₃COOH/reflux; (ii) CH₃CN/56 °C, and (iii) MeOH, CH₃COONH₄, reflux.

3.2. Electrochemical and Thermal Characterization

The electrochemical behavior of spiroopyran molecules was investigated by CV (Figure 1). In the positive scan, the CV showed an irreversible anodic trajectory because the oxidation of the indoline moiety resulted in the formation of a radical cation [2]. The oxidation peak appeared at higher potential values (E_{pa}) than those of nitrospiroopyran derivatives reported by Armendáriz-Vidales [53], demonstrating its dependence on the substituent. Substitution by a carboxylic group in para-position, unlike the results obtained by Ivashenko [54], did not show a coupling block that would prevent dimerization; therefore, we did not observe a reversible process for compound oxidation in CV [2]. As suggested by Ivashenko [54], the oxidation of the indoline nitrogen at ca. 0.91 V (E_{onset} vs. Ag/Ag^+) caused subsequent fast chemical reactions because the oxidized spiroopyran radical cation dimerized quickly by aryl C–C coupling (irreversible process). The CV curves did not exhibit a well-defined electrochemical reduction of the naphthospiroopyran. However, a cathodic signal of molecule reduction could be observed at the potential (E_{onset}) of -1.82 V vs. Ag/Ag^+ .

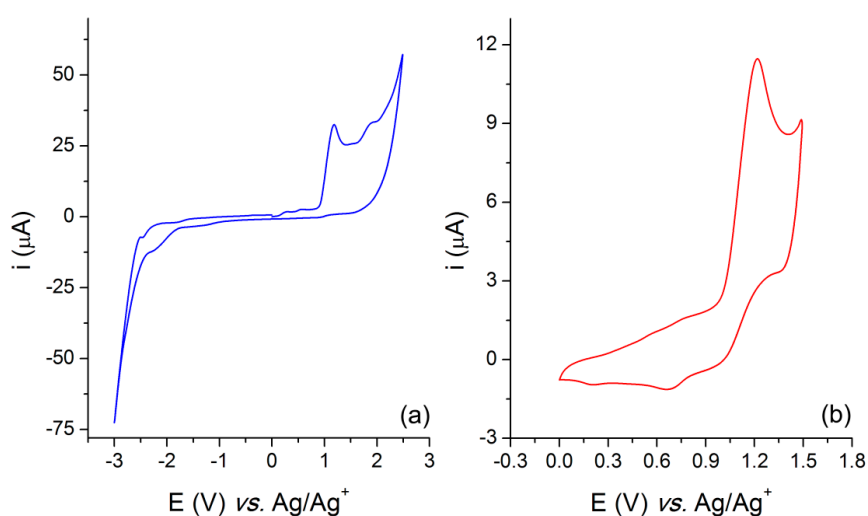


Figure 1. (a) Cyclic voltammogram of spiroopyran 7 on a glassy carbon electrode in 0.1 TBAPF₆/CH₂Cl₂ at 100 mV s⁻¹ and (b) the oxidation peak detail.

The HOMO and LUMO energy levels of π -extended conjugated molecules, like spiroopyrans, are determined by the electron affinity (EA) and ionization potential (IP) of the molecules, which could be correlated with electrochemical processes accessed by CV. In order to calculate the absolute energies, the redox data were standardized with a Fc/Fc^+ couple, and the standard reduction potential of the couple was found at 0.25 V vs. Ag/Ag^+ . The optical band gap of spiroopyran was determined from the absorption edge of its solutions. The IP value was calculated using the empirical equation $IP = -(E_{oxi}^{onset} + 4.44)$ eV, where E_{oxi}^{onset} represents the oxidation onset potential, which was 0.91 V vs. Ag/Ag^+ for the spiroopyran, and therefore a potential of 1.17 V vs. the normal hydrogen electrode (NHE). Thus, the calculated IP was equal to -5.61 eV. The EA value was obtained by subtracting the IP energy from the optical band gap, which was on the low energetic edge of the absorption spectrum ($E_{gap}^{opt} = 3.72$ eV). Therefore, the calculated EA was -1.89 eV. These electrochemical and electronic data are summarized in Table 1.

Table 1. Electrochemical and electronic properties of spiropyran 7.

Parameters	Experimental Data
E_{oxi}^{onset} (V) ^a	1.17
E_{red}^{onset} (V) ^b	-1.54
λ_{onset} (nm) ^c	332.90
E_{gap}^{opt} (eV) ^d	3.72
IP (HOMO) (eV) ^e	-5.61
EA (LUMO) (eV) ^f	-1.89

Notes: E_{oxi}^{onset} is the onset potential of oxidation, E_{red}^{onset} is the onset potential of reduction, IP (HOMO) is the ionization potential, EA (LUMO) is the electron affinity, E_{gap}^{opt} is the band-gap, and λ_{onset} is the absorption onset wavelength. ^a E_{oxi}^{onset} (vs. NHE) = E_{oxi}^{onset} (vs. Ag/Ag⁺) + 0.25; ^b E_{red}^{onset} (vs. NHE) = E_{red}^{onset} (vs. Ag/Ag⁺) + 0.25; ^c λ_{onset} : absorption onsets wavelength; ^d Optical band gap calculated on the low energetic edge of the absorption spectrum ($E_{gap}^{opt} = 1240/\lambda_{onset}$); ^e IP = - (E_{oxi}^{onset} + 4.44) eV; ^f EA calculated from IP and E_{gap}^{opt} .

The thermal behavior of the material was investigated using TGA and DSC. The decomposition temperature (T_d) of the spiropyran 7 (corresponding to 5% weight loss) was 249 °C (Figure 2).

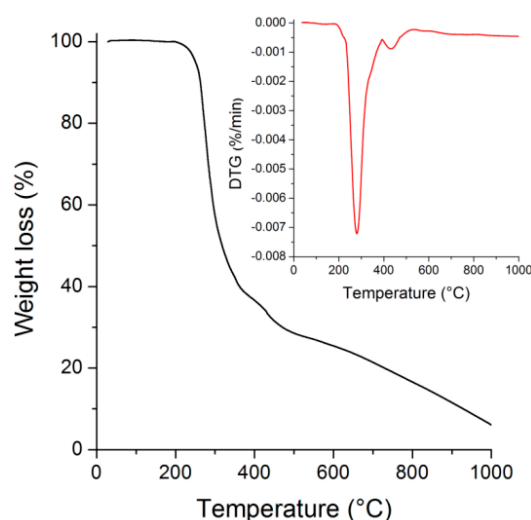


Figure 2. Thermogravimetric analysis plot of compound 7 at 10 °C·min⁻¹. The inset shows the respective derivative thermogravimetric curve.

During initial heating up to 240 °C, the compound showed endothermic peaks that corresponded to melting at approximately 242 °C (Figure S8). During cooling, the compound did not exhibit exothermic crystallization. The T_g of spiropyran was 56 °C, forming an amorphous solid at room temperature [55]. Previous studies of spiropyran derivatives with different functional groups have found lower T_m , T_g , and T_d values than those found by our research group, at 170–180 °C, 44–58 °C, and 180–200 °C, respectively [55]. Kristian et al. synthesized a series of novel spiropyran analogs with groups that possessed a C₈, C₁₂, and C₁₆ tail. The T_m of the derivatives decreased linearly with the increasing chain length, to approximately 95 °C, 85 °C, and 65 °C for the C₈, C₁₂, and C₁₆ tails, respectively. The T_m of our synthesized spiropyran was very high because of its rigid structure [56]. The results indicated that the spiropyran had a relatively high thermal stability; the relatively high T_d is crucial for the use of emissive materials in optoelectronic applications [57].

3.3. Photophysics

The photophysical investigation of the ground and excited states in solution was performed in different organic solvents (10⁻⁵ M) with a wide range of dielectric constants; the relevant data are summarized in Table 2. Figure 3 shows the UV-Vis spectra of the synthesized spiropyran, where a

sharp absorption peak at 250–350 nm can be observed with a maximum at approximately 300 nm. Moreover, we could hardly observe a solvatochromic effect ($\Delta\lambda_{\text{abs}} = 3$ nm). In addition, the molar absorptivity coefficient (ϵ) obtained by UV-Vis spectroscopy was used to calculate the oscillator strength (f_e) and the theoretical rate constant for emission (k_e^0) from the Strickler–Berg relations, presented in Equations (1) and (2), respectively [58]. Moreover, we can obtain the theoretical rate constant for emission (k_e^0) from Equation (2), and consequently, the pure radiative lifetime τ^0 , defined as $1/k_e^0$ [59].

$$f_e \approx 4.3 \times 10^{-9} \int \epsilon d\bar{\nu}, \quad (1)$$

$$k_e^0 \approx 2.88 \times 10^{-9} \bar{\nu}_0^2 \int \epsilon d\bar{\nu} \quad (2)$$

Table 2. Photophysical data of compound 7 from UV-Vis absorption, steady-state fluorescence emission, and excitation spectroscopies.

Solvent	λ_{abs}	ϵ	f	k_e^0	τ^0	$\lambda_{\text{exc}}^{\text{a)}$	$\lambda_{\text{em}}^{\text{b)}$	$\Delta\lambda_{\text{ST}}$	QY
Dichloromethane	299	2.49	0.62	6.93	1.44	319	358	59/5512	0.4
Methanol	296	2.33	0.61	7.01	1.43	321	367	71/6536	0.4
Acetonitrile	298	2.42	0.57	6.41	1.56	317	359	61/5702	0.4
Dimethylsulfoxide	298	2.21	0.60	6.73	1.49	321	359	61/5702	0.5

Note: λ_{abs} , λ_{em} , and λ_{exc} are the absorption, emission, and excitation maxima (nm), ϵ is the molar extinction coefficient ($\times 10^4 \text{ M}^{-1} \cdot \text{cm}^{-1}$), f is the calculated oscillator strength, k_e^0 is the calculated radiative rate constant (10^8 s^{-1}), τ^0 is the calculated pure radiative lifetime (ns), $\Delta\lambda_{\text{ST}}$ is the Stokes shift (nm/cm $^{-1}$), and QY is the fluorescence quantum yield (%). ^{a)} Obtained from the excitation spectra. ^{b)} Obtained using the absorption maxima as excitation wavelengths.

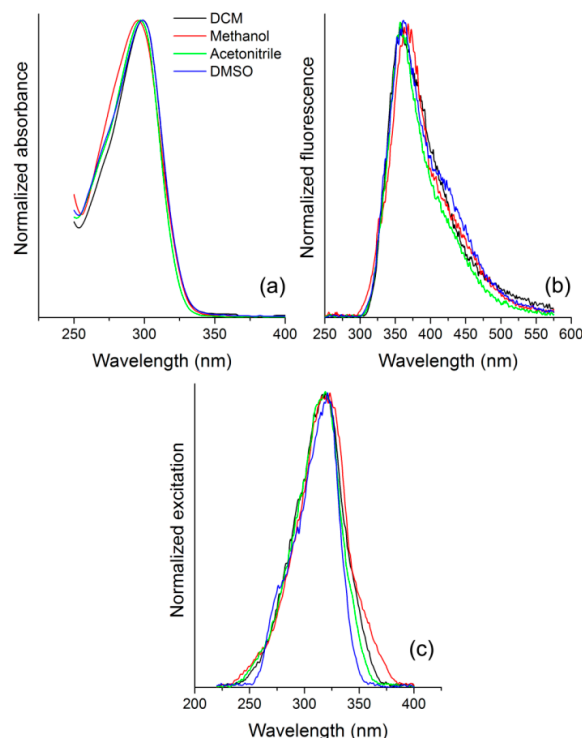


Figure 3. (a) UV-Vis absorption, (b) steady-state fluorescence emission, and (c) excitation spectra in solution of different organic solvents of spiropyran 7 [ca. 10^{-5} M] (DCM is dichloromethane, and DMSO is dimethylsulfoxide.).

The molar absorptivity coefficient (ϵ) ($\times 10^4 \text{ M}^{-1} \cdot \text{cm}^{-1}$), as well as the calculated radiative rate constants (k_e^0) (10^8 s^{-1}), indicated fully spin- and symmetry-allowed electronic transitions, that could be related to $^1\pi\pi^*$ transitions (Table 2). In addition, the oscillator strength (f) (~ 0.5) indicated highly

probable electronic transitions. The comparable constant radiative lifetime τ^0 also indicated that both absorptions populated the same excited state.

It is worth to mention that an observation of the full UV-Vis spectra (220–600 nm) did not indicate the presence of a merocyanine-like structure in these conditions (Figure S9) [1]. So, in order to study the photoisomerization ability of the synthesized compound, UV-Vis spectra were collected after continuous UV irradiation at 300 nm and 365 nm in two different ways: (i) one spectrum after 5 min of irradiation (Figure 4a,b), and (ii) one every 2 min for 50 min (Figure 4c,d). All spectra presented an absorption maximum at 300 nm, ascribed to the closed-form (lower conjugation), as already observed in similar spiropyran dyes [1,2]. However, and surprisingly, no additional redshifted absorption bands could be observed under any circumstances in this compound. The literature relates that under UV radiation, the spiro form, which is colorless presents a carbon-oxygen bond cleavage of the pyran ring, followed by *cis-trans* isomerization to reach the colored merocyanine (MC) form [60]. The MC form (open-form) is highly conjugated, presenting an absorption band in the visible region. In addition, it is reported in the literature that the open-form can be stabilized by the nitro group in the para position to the phenolic oxygen [61]. In this way, and based on the results presented in Figure 4, no evidence of an open form could be observed in this study, which may be related to the absence of the electron-withdrawing nitro group that cannot stabilize the generated phenolate as a weak base.

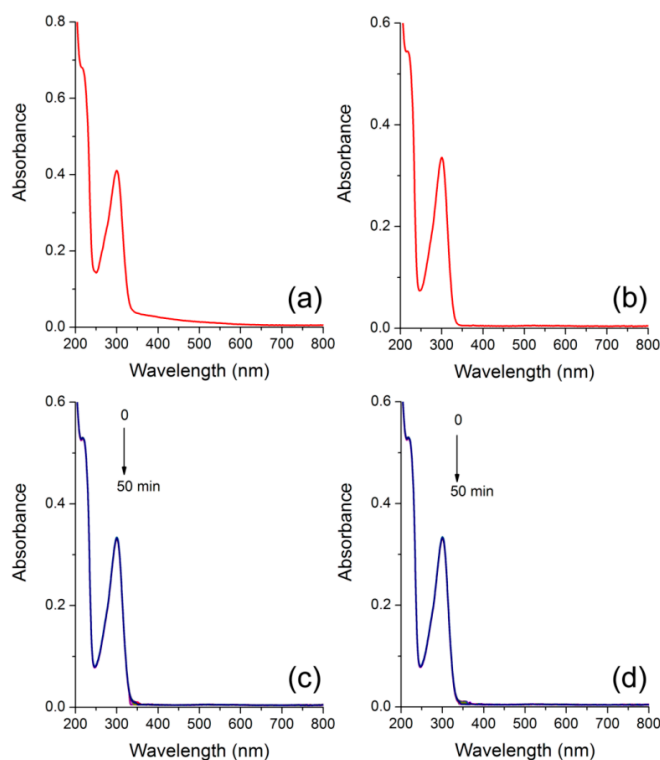


Figure 4. UV-Vis absorbance spectra of spiropyran 7 [10^{-5} mol·L $^{-1}$] in acetonitrile solution, at (a) 300 nm and (b) 365 nm irradiation for 5 min, and at (c) 300 nm and (d) 365 nm irradiation every 2 min for 50 min.

The fluorescence emission spectra were obtained by exciting the compound at the absorption maxima and the excitation spectra were obtained using the fluorescence emission maxima as observation wavelength (λ_{exc}). The respective spectra in different solvents are also presented in Figure 3, and the data are summarized in Table 2. The spiropyran showed a main fluorescence emission at approximately 360 nm with a Stokes shift of approximately 5600 cm^{-1} . Based on the photoisomerization experiment, the emission was related to the closed form of this compound. The observed fluorescence maxima obtained from the excitation spectra could be related to this species, as well.

3.4. Ionization Constants

The determination of the ionization constants of the synthesized spiropyran plays a fundamental role in this investigation since the molecule contains an additional carboxyl moiety, which can influence its photochromic properties. In this sense, the pK_a values were obtained in 1:1 EtOH/H₂O solution (v/v) applying the Henderson–Hasselbach relation, presented in Equation (3):

$$pH = pK_a + \log \frac{(A - A_a)}{(A_b - A)}, \quad (3)$$

where A_a is the absorbance of the protonated specie, A_b is the absorbance of the neutral specie and A is the absorbance of both the protonated and neutral species in the solution [34,35]. Experimentally, it is performed by measuring the absorbance of anionic, neutral (using KOH) and protonated (using HCl) species at a specific absorption wavelength as a function of the pH [34,35]. In this procedure, the determination of the ionization constants depends on the direct determination of the ratio of molecular (neutral) to ionized (protonated) species in non-absorbing solutions, whose pH values are measured. In this way, to optimize the optical response, a specific wavelength was chosen, at which the greatest difference between the absorbances of the two species is observed. In addition, the acidic strength of the phenolic hydrogen in water in the electronic ground state (${}_w pK_a$) was obtained by extrapolation [62–65].

Figure 5 presents the UV-Vis absorption spectra of the spiropyran in solution and the dependence on the absorbance intensity vs. pH. In this curve, the variation of the absorbance intensities is due to the presence of both neutral and deprotonated species at the relevant pH values. It can be observed that the absorptions in the UV region of the neutral, first, and second deprotonated species are located at 300 nm, 290 nm, and 270 nm, respectively. Therefore, the wavelength of 277 nm was the most suitable to determine its pK_a. The results could be fitted using a sigmoidal curve, where the inflection points were determined at 3.40 and 10.81. According to Equation (3), the pH is equal to pK_a at the inflection points. A plateau can be found at pH lower than 4.0, between 4 and 8, and higher than 12. These preliminary results indicated that spiropyran is a potential candidate for sensing pH in the UV region.

Previous studies suggest that nitro group-substituted spiropyrans favor the formation of the merocyanine form in acidic media [1]; however, other studies propose that this opening is favored in strongly basic media [66]. The studied compound exhibits similar behavior to that observed by Zheng et al. [62], where the closed structure is favored in acidic pH, while the open form (merocyanine) is favored in basic media. Moreover, the synthesized carboxylic derivative shows a blueshift in its merocyanine form, unlike the redshift of derivatives containing electron withdrawal groups (EWG), such as nitro and cyano groups [1,61,62,67]. This behavior shows that both the absence of these EWG and the presence of the carboxyl moiety in the indolic ring plays a key role in the species equilibrium and modulate their absorption spectra. In addition, as already discussed, we determined the ionization constant in water (${}_w pK_a$) from the measured pK_a in the ethanol/water solution (1:1 v/v) using the relationship $pK_a = {}_w pK_a - d$, where d is 0.21 in the same solution with 0.1 ionic strength (KCl solution of 0.15 mol·L⁻¹) [68]. The pK_a values in water were 3.40 and 10.81, and attributed to the carboxylic acid and phenol groups ionization of the spiropyran, respectively.

3.5. BSA Interaction Study

It is well known that BSA in a buffered solution exhibits UV-Vis absorption and intrinsic fluorescence emission located at 280 nm and 340 nm, respectively, due to tryptophan residues [69]. Its fluorescence suppression can be a powerful tool to elucidate its interaction with small molecules, since BSA is largely used as protein model. In this way, it was studied the interaction of BSA with the spiropyran on suppression experiments, where the BSA concentration was kept constant (7.33 mM), and the concentration of the spiropyran changed from 1.9 mM up to 20.0 mM (Figure 6).

Conversely, the interaction of spiropyran with the BSA was studied in association experiments. However, no association of the spiropyran with BSA related to the increase in the fluorescence intensity of the precursors could be observed.

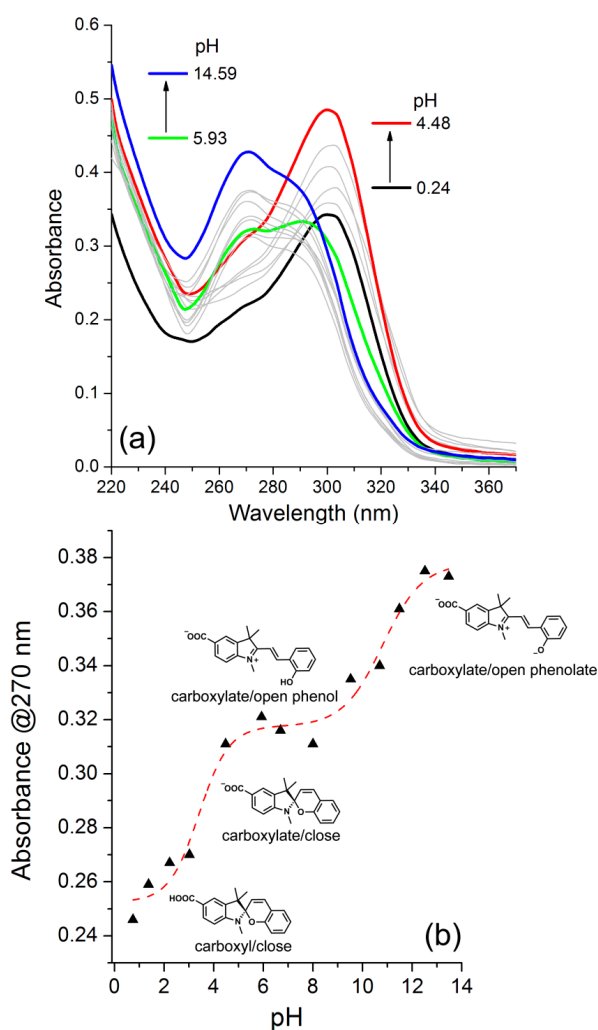


Figure 5. (a) UV-Vis absorption spectra of spiropyran in ethanol/water solution (1:1 *v/v*) in indicated pH values at 25 °C and (b) dependence on the absorbance intensity vs. pH recorded at 270 nm. The dotted line was fitted according to the Boltzmann sigmoidal curve function.

Upon the addition of spiropyran into the solution containing bovine serum albumin, the absorption band located at approximately 279 nm increased (BSA absorption band), as expected. Additionally, a decrease in the fluorescence intensity of the BSA took place after the addition of spiropyran. Based on these results, the observed BSA fluorescence quenching was quantitatively evaluated using the collisional Stern–Volmer relation, presented in Equation (4) [70].

$$F_0/F = 1 + K_{SV} [Q] = 1 + K_q \tau_0 [Q], \quad (4)$$

where F_0 and F are the fluorescence intensities of the BSA in the absence and presence of the spiropyran, respectively; $[Q]$ is the spiropyran concentration; K_{SV} is the Stern–Volmer constant, and is the product of a bimolecular suppression constant K_q and the fluorophore lifetime ($\tau_0 \sim 10^{-9}$ s) in the absence of the quencher [66]. Thus, we determined a linear plot correlation ($F_0/F = 0.987 + 73\,377.83 [Q]$, R-Square: 0.992) and calculated the K_{SV} at $7.33 \times 10^4 \text{ M}^{-1}$. Additionally, the bimolecular suppression constant K_q for BSA was calculated at $7.33 \times 10^{13} \text{ M}^{-1} \cdot \text{s}^{-1}$ based on τ_0 , which exceeded the maximum values

of the diffusional mechanism ($2.0 \times 10^{-1} \cdot \text{s}^{-1}$). Thus, the nature of quenching was not dynamic but static suppression, resulting in the formation of spiropyran-BSA complexes in the ground state [71]. Moreover, we could calculate the binding constant (K_a) and the respective number of binding sites (n) between the BSA and the spiropyran by applying the Scatchard relation, presented in Equation (5) [72]:

$$\log [(F_0 - F)/F] = \log K_a + n \log [Q], \quad (5)$$

Figure 7 exhibits the double logarithmic plot of the fluorescence intensities of BSA over the spiropyran concentration. We observe a linear plot correlation ($\log [(F_0 - F)/F] = 4.89289 + 1.00695 \log [Q]$, R-Square: 0.964) with comparable binding constants (K_a) of 7.81×10^4 with one binding site ($n \sim 1$), indicating a non-significant role in the interaction of spiropyran with the BSA.

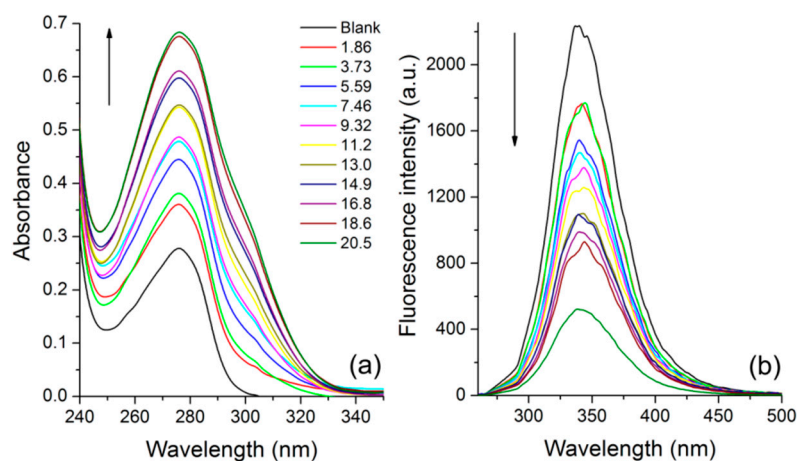


Figure 6. UV-Vis absorption (a) and fluorescence emission (b) spectra ($\lambda_{\text{exc}} = 279$ nm) of BSA in PBS solution (7.33 mM) in the presence of different amounts of spiropyran (10^{-5} M). The blank sample is pure BSA.

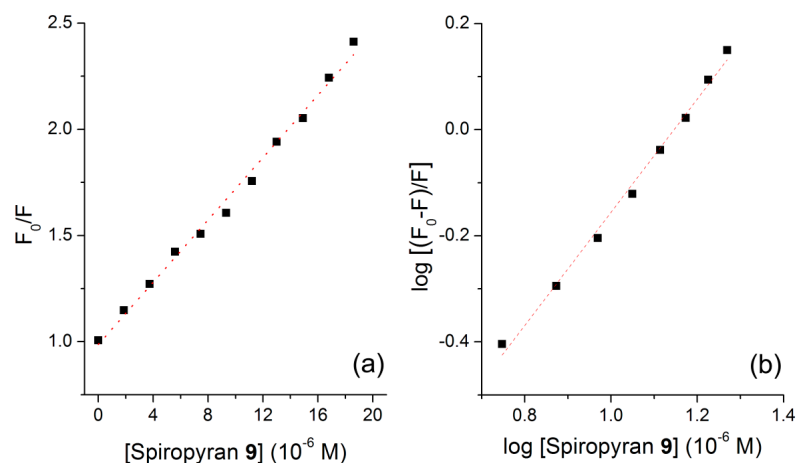


Figure 7. Stern–Volmer equation plots of BSA fluorescence intensity vs. spiropyran concentration in the suppression experiment (a) and log-log plot of BSA fluorescence intensity vs. spiropyran concentration (b) used to obtain the binding constant (K_a) and binding sites (n) from Equation (5).

3.6. Theoretical Calculation

The ground (S_0) and first (S_1) excited state in dichloromethane obtained at PBE1PBE/cc-pVDZ level of theory is shown in Figure 8. All obtained geometries were very similar for all solvents, both in the ground and the first excited state (Figure S10). In the S_1 , the geometry of spiropyran is quite similar to the ground state; however, in the excited state there is an approximation of the indol and the

benzopyran rings with the OCN angle going from $\sim 110^\circ$ to $\sim 106^\circ$. The theoretical photophysical data obtained at PBE1PBE/jun-cc-pVTZ level of theory are shown in Table 3.

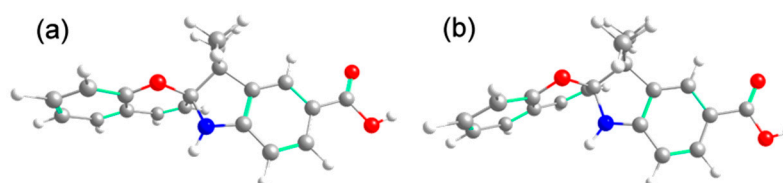


Figure 8. Geometries in the ground (a) and the first excited state (b) of spiroopyran 7 obtained at PBE1PBE/cc-pVDZ level of theory in dichloromethane.

Table 3. Calculated photophysical properties of spiroopyran 7 at PBE1PBE/jun-cc-pVTZ level of theory.

Solvent	λ_{abs}	Δ_{abs}	μ_{GS}	f	λ_{em}	f	Δ_{em}	μ_{ES}	$\Delta\lambda_{\text{ST}}$
Dichloromethane	309	10	4.81	0.7811	402	0.1832	44	11.37	7487
Acetonitrile	311	13	4.99	0.8724	395	0.2407	36	11.31	6838
Methanol	311	15	4.99	0.8694	395	0.2384	32	11.31	6838

Note: λ_{abs} and λ_{exc} are the absorption and emission wavelengths (nm), Δ_{abs} and Δ_{em} are the absolute difference between the experimental and the theoretical wavelengths, μ_{GS} and μ_{ES} are the dipole moments of the ground state and excited state respectively, f is the oscillator strength and $\Delta\lambda_{\text{ST}}$ is the Stokes shift (cm^{-1}).

After excitation, the first excited state is populated due to its high oscillator strength in comparison to others computed excited states. This $S_0 \rightarrow S_1$ transition only occurs between the HOMO and LUMO orbitals, HOMO a π orbital and LUMO an π^* orbital, making the $S_0 \rightarrow S_1$ transition have a $^1\pi\pi^*$ character (Figure 9). Similar results could be observed in acetonitrile and methanol (Figure S11). The experimental data shows that methanol and acetonitrile had lower absorption wavelengths (296 nm and 298 nm, respectively) than dichloromethane (299 nm). However, this behavior is not observed in the TD-DFT results, as the theoretical absorption wavelengths for dichloromethane is lower in comparison to methanol and acetonitrile. This is because PCM only simulates solvent effects implicitly, and thus is not capable to take into account explicit solvent–solute interactions, e.g., hydrogen bonds between polar groups of spiroopyran and solvent. In the theoretical data is observed a small increase in the absorption wavelengths with the increase of the dielectric constant, because the polarity of spiroopyran increases in the excited state.

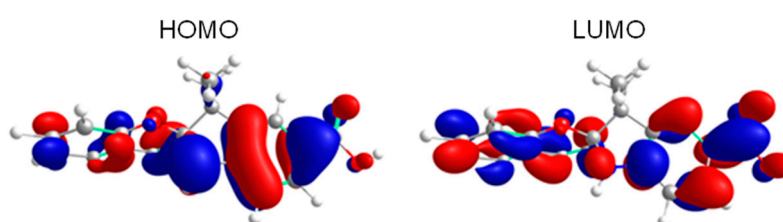


Figure 9. HOMO and LUMO orbitals involved in the $S_0 \rightarrow S_1$ transition of spiroopyran 7 obtained at PBE1PBE/jun-cc-pVTZ level of theory in dichloromethane.

It was also investigated if the spiroopyran 7 shows intramolecular charge transfer (ICT). The depletion region (C-), representing the decrease of electronic density that after excitation, and the increment region (C+), representing the increase of electronic density after excitation, are shown in Figure 10 for dichloromethane, acetonitrile and methanol. Evaluating the D_{CT} values, a measure of the distance of the barycenter of the depletion and increment regions, in dichloromethane, 1.33 Å, acetonitrile, 0.91 Å, and methanol, 0.93 Å it is concluded that spiroopyran shows ICT for all considered solvents, with the largest distance between the two regions being observed on dichloromethane. In the $S_0 \rightarrow S_1$ transition there is an electronic density transfer of the indole ring to the benzopyran ring.

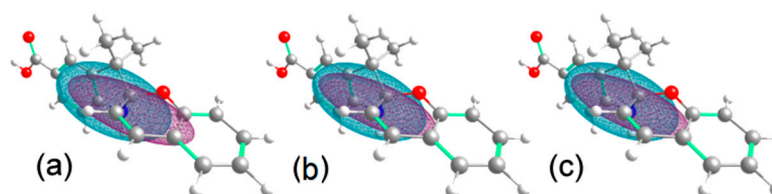


Figure 10. Depletion (blue) and increment (purple) regions for spiroopyran 7 in dichloromethane (a), acetonitrile (b) and methanol (c) for the $S_0 \rightarrow S_1$ transition.

4. Conclusions

We synthesized and characterized a novel spiroopyran to investigate its relationship with BSA and elucidate its physical properties. The spiroopyran presented an intense band at approximately 300 nm related to the $\pi-\pi^*$ electronic transitions from the ground state to the first excited state. The obtained Strickler–Berg parameters corroborate these observations. The synthesized spiroopyran presented a single fluorescence emission band at approximately 558 nm. The difference found between the experimental and theoretical results can be explained by the fact that PCM simulates the solvent effect implicitly and not explicitly. The $S_0 \rightarrow S_1$ transition show a ${}^1\pi\pi^*$ character involving the HOMO and LUMO orbitals. The calculated D_{CT} values shows that spiroopyran exhibit ICT. The values of the ionization constant in water were 3.40 and 10.81, and attributed to the ionization of the carboxylic acid and phenol group of the spiroopyran, respectively. Despite the absence of photoisomerization, we studied the interaction of this compound with BSA successfully, and it showed suppression properties, with relatively large Stern–Volmer values ($\sim 10^4 M^{-1}$) and bimolecular suppression ($\sim 10^{13} M^{-1}\cdot s^{-1}$) constants. Steady-state experiments indicated that the nature of the suppression was static.

Supplementary Materials: The Supplementary Materials are available online at <http://www.mdpi.com/2227-9040/8/2/31/s1>. Figure S1: 1H NMR spectrum of compound 3 in $CDCl_3$ (300 MHz), Figure S2: ${}^{13}C$ NMR spectrum of compound 3 in $CDCl_3$ (75 MHz), Figure S3: 1H NMR spectrum of compound 5 in $DMSO-d_6$ (300 MHz), Figure S4: ${}^{13}C$ NMR spectrum of compound 5 in $DMSO-d_6$ (75 MHz), Figure S5: FTIR spectrum of compound 7 in NaCl window, Figure S6: 1H NMR spectrum of compound 7 in $CDCl_3$ (400 MHz), Figure S7: ${}^{13}C$ NMR spectrum of compound 7 in $CDCl_3$ (100 MHz), Figure S8: Differential Scanning Calorimetry (DSC) plots of compound 7 measured at $10^\circ C/min$ showing the glass transition temperature (T_g) and melting point temperature (T_m), Figure S9: Full UV-Vis spectra in solution of compound 7 different organic solvents [ca. $10^{-5} M$], Figure S10: Geometries of spiroopyran in acetonitrile and methanol, Figure S11: HOMO and LUMO orbitals in acetonitrile and methanol.

Author Contributions: R.d.C.D. and F.d.S.S. contributed with conception and design of the study; F.S.R. established the specific methodology; R.d.C.D., F.d.S.S. and R.C. organized the database; R.d.C.D., F.d.S.S. and R.C. performed the synthesis, analyses and investigations; D.B. and E.Z. performed and validated the electrochemical experiments; A.G.D.-B. provided resources; R.d.C.D., F.d.S.S. and R.C. wrote the first draft of the manuscript; F.S.R. and A.G.D.-B. supervised final editing and managed project; B.B.d.A. and P.F.B.G. performed and validated the theoretical calculations. All authors have read and agreed to the published version of the manuscript.

Funding: This research was funded by National Council for Scientific and Technological Development – CNPq, grant number 305954/2019-9, Coordenação de Aperfeiçoamento de Pessoal de Nível Superior - Brasil (CAPES) - Finance Code 001 and CELESC P&D grant number 05697-1718/2018 and 5697-0717/2017.

Acknowledgments: The authors thank Teresa Dib Zambon Atvars and Luís Gustavo Teixeira Alves for the photoisomerization study.

Conflicts of Interest: The authors declare that the research was conducted in the absence of any commercial or financial relationships that could be construed as a potential conflict of interest.

References

1. Klajn, R. Spiroopyran-based dynamic materials. *Chem. Soc. Rev.* **2014**, *43*, 148–184. [[CrossRef](#)] [[PubMed](#)]
2. Kortekaas, L.; Browne, W.R. The evolution of spiroopyran: fundamentals and progress of an extraordinarily versatile photochrome. *Chem. Soc. Rev.* **2019**, *48*, 3406–3424. [[CrossRef](#)] [[PubMed](#)]
3. Feeney, M.J.; Thomas, S.W. Tuning the Negative Photochromism of Water-Soluble Spiroopyran Polymers. *Macromol.* **2018**, *51*, 8027–8037. [[CrossRef](#)]

4. Li, X.; Li, J.; Wang, Y.; Matsuura, T.; Meng, J.-B. Synthesis of functionalized spiropyran and spirooxazine derivatives and their photochromic properties. *J. Photochem. Photobiol. A: Chem.* **2004**, *161*, 201–213. [[CrossRef](#)]
5. Samanta, D.; Galaktionova, D.; Gemen, J.; Shimon, L.J.W.; Diskin-Posner, Y.; Avram, L.; Král, P.; Klajn, R. Reversible chromism of spiropyran in the cavity of a flexible coordination cage. *Nat. Commun.* **2018**, *9*, 641. [[CrossRef](#)] [[PubMed](#)]
6. Huang, C.-Q.; Wang, Y.; Hong, C.-Y.; Pan, C.-Y. Spiropyran-Based Polymeric Vesicles: Preparation and Photochromic Properties. *Macromol. Rapid Commun.* **2011**, *32*, 1174–1179. [[CrossRef](#)]
7. Chan, Y.-H.; Gallina, M.E.; Zhang, X.; Wu, I.-C.; Jin, Y.; Sun, W.; Chiu, D.T. Reversible Photoswitching of Spiropyran-Conjugated Semiconducting Polymer Dots. *Anal. Chem.* **2012**, *84*, 9431–9438. [[CrossRef](#)]
8. Cui, L.; Zhang, H.; Zhang, G.; Zhou, Y.; Fan, L.; Shi, L.; Zhang, C.; Shuang, S.; Dong, C. Substituent effect on the acid-induced isomerization of spiropyran compounds. *Spectrochim. Acta Part A: Mol. Biomol. Spectrosc.* **2018**, *202*, 13–17. [[CrossRef](#)]
9. Byrne, R.; Fraser, K.J.; Izgorodina, E.; Macfarlane, D.R.; Forsyth, M.; Diamond, D. Photo- and solvatochromic properties of nitrobenzospiroxyran in ionic liquids containing the [NTf₂][−] anion. *Phys. Chem. Chem. Phys.* **2008**, *10*, 5919–5924. [[CrossRef](#)]
10. Crano, J.C.; Guglielmetti, R.J. (Eds.) *Organic photochromic and thermochromic compounds*, 1st ed.; Springer US: New York, NY, USA, 2002.
11. Kobatake, S.; Irie, M. 8 Photochromism. *Annu. Rep. Prog. Chem. Sect. C: Phys. Chem.* **2003**, *99*, 277–313. [[CrossRef](#)]
12. Paramonov, S.; Lokshin, V.; Fedorova, O.A. Spiropyran, chromene or spirooxazine ligands: Insights into mutual relations between complexing and photochromic properties. *J. Photochem. Photobiol. C: Photochem. Rev.* **2011**, *12*, 209–236. [[CrossRef](#)]
13. Berkovic, G.; Krongauz, V.; Weiss, V. Spiroxyrans and Spirooxazines for Memories and Switches. *Chem. Rev.* **2000**, *100*, 1741–1754. [[CrossRef](#)] [[PubMed](#)]
14. Levitus, M.; Glasser, G.; Neher, D.; Aramendía, P.F. Direct measurement of the dipole moment of a metastable merocyanine by electromechanical interferometry. *Chem. Phys. Lett.* **1997**, *277*, 118–124. [[CrossRef](#)]
15. Bletz, M.; Pfeifer-Fukumura, U.; Kolb, U.; Baumann, W. Ground- and First-Excited-Singlet-State Electric Dipole Moments of Some Photochromic Spirobenzopyrans in Their Spiropyran and Merocyanine Form†. *J. Phys. Chem. A* **2002**, *106*, 2232–2236. [[CrossRef](#)]
16. Casades, I.; Constantine, S.; Cardin, D.; García, H.; Gilbert, A.; Márquez, F. ‘Ship-in-a-Bottle’ Synthesis and Photochromism of Spiroxyrans Encapsulated within Zeolite Y Supercages. *Tetrahedron* **2000**, *56*, 6951–6956. [[CrossRef](#)]
17. Alonso, M.; Rebotto, V.; Guiscardo, L.; Martin, A.S.; Rodríguez-Cabello, J.C. Spiropyran Derivative of an Elastin-like Bioelastic Polymer: Photoresponsive Molecular Machine to Convert Sunlight into Mechanical Work. *Macromol.* **2000**, *33*, 9480–9482. [[CrossRef](#)]
18. Xia, H.; Chen, Y.; Yang, G.; Zou, G.; Zhang, Q.; Zhang, D.; Wang, P.; Ming, H. Optical Modulation of Waveguiding in Spiropyran-Functionalized Polydiacetylene Microtube. *ACS Appl. Mater. Interfaces* **2014**, *6*, 15466–15471. [[CrossRef](#)]
19. Shiraishi, Y.; Shirakawa, E.; Tanaka, K.; Sakamoto, H.; Ichikawa, S.; Hirai, T. Spiropyran-Modified Gold Nanoparticles: Reversible Size Control of Aggregates by UV and Visible Light Irradiations. *ACS Appl. Mater. Interfaces* **2014**, *6*, 7554–7562. [[CrossRef](#)]
20. Tian, W.; Tian, J. Synergy of Different Fluorescent Enhancement Effects on Spiropyran Appended onto Cellulose. *Langmuir* **2014**, *30*, 3223–3227. [[CrossRef](#)]
21. Schenderlein, H.; Voss, A.; Stark, R.W.; Biesalski, M. Preparation and Characterization of Light-Switchable Polymer Networks Attached to Solid Substrates. *Langmuir* **2013**, *29*, 4525–4534. [[CrossRef](#)]
22. Shiraishi, Y.; Miyamoto, R.; Hirai, T. Spiropyran-Conjugated Thermoresponsive Copolymer as a Colorimetric Thermometer with Linear and Reversible Color Change. *Org. Lett.* **2009**, *11*, 1571–1574. [[CrossRef](#)] [[PubMed](#)]
23. Sheng, L.; Li, M.; Zhu, S.; Li, H.; Xi, G.; Li, Y.-G.; Wang, Y.; Li, Q.; Liang, S.; Zhong, K.; et al. Hydrochromic molecular switches for water-jet rewritable paper. *Nat. Commun.* **2014**, *5*, 3044. [[CrossRef](#)] [[PubMed](#)]
24. Wan, S.; Zheng, Y.; Shen, J.; Yang, W.; Yin, M. “On-off-on” Switchable Sensor: A Fluorescent Spiropyran Responds to Extreme pH Conditions and Its Bioimaging Applications. *ACS Appl. Mater. Interfaces* **2014**, *6*, 19515–19519. [[CrossRef](#)] [[PubMed](#)]

25. Abdollahi, A.; Alinejad, Z.; Mahdavian, A.R. Facile and fast photosensing of polarity by stimuli-responsive materials based on spiropyran for reusable sensors: a physico-chemical study on the interactions. *J. Mater. Chem. C* **2017**, *5*, 6588–6600. [CrossRef]
26. Parker, R.; Gates, J.; Rogers, H.L.; Smith, P.; Grossel, M.C. Using the photoinduced reversible refractive-index change of an azobenzene co-polymer to reconfigure an optical Bragg grating. *J. Mater. Chem.* **2010**, *20*, 9118–9125. [CrossRef]
27. Xu, Z.; Li, S.; Shen, Y.; Chen, M.; Shao, X. Spiropyran-azobenzene-DBU system as solvent indicator. *Tetrahedron Lett.* **2018**, *59*, 3829–3832. [CrossRef]
28. Chen, J.; Xu, L.; Wu, S.; Su, J.; Tong, Z. Photoreversible Fluorescent Modulation of Nanoparticles via One-Step Miniemulsion Polymerization. *Small* **2009**, *5*, 970–978. [CrossRef]
29. Cui, H.; Liu, H.; Chen, S.; Wang, R. Synthesis of amphiphilic spiropyran-based random copolymer by atom transfer radical polymerization for Co²⁺ recognition. *Dye. Pigment.* **2015**, *115*, 50–57. [CrossRef]
30. Streib, M.; Kräling, K.; Richter, K.; Xie, X.; Steuber, H.; Meggers, E. An organometallic inhibitor for the human repair enzyme 7,8-dihydro-8-oxoguanosine triphosphatase. *Angew. Chem. Int. Ed.* **2014**, *53*, 305–309. [CrossRef]
31. Wang, L.-F.; Chen, J.-W.; Chen, J.-W. Cyclodextrin effects on the photochromism of spiropyran/β-cyclodextrin inclusion polymers. *Mater. Chem. Phys.* **2012**, *136*, 151–159. [CrossRef]
32. Raymo, F.M.; Alvarado, R.J.; Giordani, S.; Cejas, M.A. Memory Effects Based on Intermolecular Photoinduced Proton Transfer. *J. Am. Chem. Soc.* **2003**, *125*, 2361–2364. [CrossRef] [PubMed]
33. Zhu, M.-Q.; Zhang, G.-F.; Li, C.; Aldred, M.; Chang, E.; Drezek, R.A.; Li, A.D.Q. Reversible Two-Photon Photoswitching and Two-Photon Imaging of Immunofunctionalized Nanoparticles Targeted to Cancer Cells. *J. Am. Chem. Soc.* **2011**, *133*, 365–372. [CrossRef] [PubMed]
34. Wang, Y.; Xu, Z.; Dai, X.; Li, H.; Yu, S.; Meng, W. A New Spiropyran-Based Sensor for Colorimetric and Fluorescent Detection of Divalent Cu²⁺ and Hg²⁺ Ions and Trivalent Ce³⁺, Cr³⁺ and Al³⁺ Ions. *J. Fluoresc.* **2019**, *29*, 569–575. [CrossRef] [PubMed]
35. Lafuma, A.; Quinn, F.X.; Sanchez, C.; Chodorowski-Kimmes, S. Photochromic Properties of a Spirooxazine and a Spiropyran in Alcoholic Solutions of Zirconium and Aluminium Alkoxides: Influence of the Ethyl Acetoacetate Chelating Agent on the Optical Properties. *Eur. J. Inorg. Chem.* **2003**, *2003*, 331–338. [CrossRef]
36. Lee, C.H.; Yun, H.J.; Jung, M.R.; Lee, J.G.; Kim, J.H.; Kim, J.H. Preparation and Characterization of Squaraine Dyes containing Mono- and Bis-Anchoring Groups as the Light Absorber in Dye Sensitized Solar Cells. *Electrochimica Acta* **2014**, *138*, 148–154. [CrossRef]
37. Armarego, W.L.F.; Chai, C. *Purification of Laboratory Chemicals*, 7th ed.; Butterworth-Heinemann: Oxford, UK, 2013.
38. Würth, C.; Grabolle, M.; Pauli, J.; Spieles, M.; Resch-Genger, U. Relative and absolute determination of fluorescence quantum yields of transparent samples. *Nat. Protoc.* **2013**, *8*, 1535–1550. [CrossRef]
39. Avdeef, A.; Comer, J.E.A.; Thomson, S.J. pH-Metric log P. 3. Glass electrode calibration in methanol-water, applied to pK_a determination of water-insoluble substances. *Anal. Chem.* **1993**, *65*, 42–49. [CrossRef]
40. Herrero-Martínez, J.M.; Repollés, C.; Bosch, E.; Rosés, M.; Ràfols, C. Potentiometric determination of aqueous dissociation constants of flavonols sparingly soluble in water. *Talanta* **2008**, *74*, 1008–1013. [CrossRef]
41. Duarte, L.G.T.A.; Germino, J.C.; de Ávila Braga, C.; Barboza, C.A.; Atvars, T.D.Z.; Santos, F.D.S.; Rodembusch, F.S. Photoacidity as a tool to rationalize excited state intramolecular proton transfer reactivity in flavonols. *Photochem. Photobiol. Sci.* **2018**, *17*, 231–238. [CrossRef]
42. Coelho, F.L.; de Ávila Braga, C.; Zanotto, G.M.; Gil, E.S.; Campo, L.F.; Gonçalves, P.F.B.; Rodembusch, F.S.; Santos, F.D.S. Low pH optical sensor based on benzothiazole azo dyes. *Sensors Actuators B: Chem.* **2018**, *259*, 514–525. [CrossRef]
43. Castro, G.T.; Giordano, O.S.; Blanco, S.E. Determination of the pK_a of hydroxy-benzophenones in ethanol-water mixtures. Solvent effects. *J. Mol. Struct. THEOCHEM* **2003**, *626*, 167–178. [CrossRef]
44. Frisch, M.J.; Trucks, G.W.; Schlegel, H.B.; Scuseria, G.E.; Robb, M.A.; Cheeseman, J.R.; Scalmani, G.; Barone, V.; Petersson, G.A.; Nakatsuji, H.; et al. *Gaussian 16, Revision A.03*; Gaussian, Inc.: Wallingford, CT, USA, 2016; Available online: <https://gaussian.com/> (accessed on 29 April 2020).
45. Ernzerhof, M.; Scuseria, G.E. Assessment of the Perdew–Burke–Ernzerhof exchange-correlation functional. *J. Chem. Phys.* **1999**, *110*, 5029–5036. [CrossRef]

46. Papajak, E.; Zheng, J.; Xu, X.; Leverentz, H.R.; Truhlar, D. Perspectives on Basis Sets Beautiful: Seasonal Plantings of Diffuse Basis Functions. *J. Chem. Theory Comput.* **2011**, *7*, 3027–3034. [CrossRef] [PubMed]
47. Tomasi, J.; Mennucci, B.; Cammi, R. Quantum Mechanical Continuum Solvation Models. *ChemRev* **2005**, *36*, 2999–3093. [CrossRef]
48. Le Bahers, T.; Adamo, C.; Ciofini, I. A Qualitative Index of Spatial Extent in Charge-Transfer Excitations. *J. Chem. Theory Comput.* **2011**, *7*, 2498–2506. [CrossRef]
49. Lu, T. Computer Program, Multiwfn. 2017. Available online: <https://www.multiwfn.codeplex.com> (accessed on 24 March 2020).
50. Chemcraft - graphical software for visualization of quantum chemistry computations. Available online: <https://www.chemcraftprog.com> (accessed on 24 March 2020).
51. Allen, C.F.H.; Wilson, C. V The use of N15 as a tracer element in chemical reactions. The mechanism of the Fischer indole synthesis. *J. Am. Chem. Soc.* **1943**, *65*, 611–612. [CrossRef]
52. Zhang, X.; Heng, S.; Abell, A.D. Photoregulation of α -chymotrypsin activity by spiropyran-based inhibitors in solution and attached to an optical fiber. *Chem. Eur. J.* **2015**, *21*, 10703–10713. [CrossRef]
53. Armendáriz-Vidales, G.; Martínez-González, E.; Hernández-Melo, D.; Tiburcio, J.; Frontana, C. Electrochemical Characterization of Spiropyran Structures. *Procedia Chem.* **2014**, *12*, 41–46. [CrossRef]
54. Ivashenko, O.; Van Herpt, J.T.; Rudolf, P.; Feringa, B.L.; Browne, W.R. Oxidative electrochemical aryl C–C coupling of spiropyrans. *Chem. Commun.* **2013**, *49*, 6737–6739. [CrossRef]
55. Gerkman, M.A.; Yuan, S.; Duan, P.; Taufan, J.; Schmidt-Rohr, K.; Han, G.G.D. Phase transition of spiropyrans: impact of isomerization dynamics at high temperatures. *Chem. Commun.* **2019**, *55*, 5813–5816. [CrossRef]
56. Tangso, K.J.; Fong, W.-K.; Darwish, T.A.; Kirby, N.; Boyd, B.J.; Hanley, T.L. Novel Spiropyran Amphiphiles and Their Application as Light-Responsive Liquid Crystalline Components. *J. Phys. Chem. B* **2013**, *117*, 10203–10210. [CrossRef] [PubMed]
57. Li, X.; Li, C.; Wang, S.; Dong, H.; Ma, X.; Cao, D. Synthesis and properties of photochromic spirooxazine with aggregation-induced emission fluorophores polymeric nanoparticles. *Dye. Pigment.* **2017**, *142*, 481–490. [CrossRef]
58. Strickler, S.J.; Berg, R.A. Relationship between Absorption Intensity and Fluorescence Lifetime of Molecules. *J. Chem. Phys.* **1962**, *37*, 814–822. [CrossRef]
59. Turro, N.J.; Scaiano, J.C.; Ramamurthy, V. *Principles of molecular photochemistry: An introduction*, 1st ed.; University Science Books: Sausalito, CA, USA, 2009.
60. He, T.; Zhang, J. (Eds.) *Photochromic Materials: Preparation, Properties and Applications*, 1st ed.; Wiley-VCH: Weinheim, Germany, 2016.
61. Metelitsa, A.V.; Micheau, J.C.; Besugliy, S.O.; Gaeva, E.B.; Voloshin, N.A.; Voloshina, E.N.; Samat, A.; Minkin, V.I. Photochromic properties of six 5-On-alkyl, 6'-CN substituted spironaphthoxazines. *Int. J. Photoenergy* **2004**, *6*, 199–204. [CrossRef]
62. Tiwari, S.; Ghosh, K.K.; Marek, J.; Ramalho, T.C. Spectrophotometric Determination of the Acidity Constants of Some Oxime-Based α -Nucleophiles. *J. Chem. Eng. Data* **2010**, *55*, 1153–1157. [CrossRef]
63. Islamoglu, F.; Kahveci, B.; Ozil, M.; Akyuz, E. Studies on the protonation constants of some triazoles in ethanol-water mixtures. *Asian J. Chem.* **2008**, *20*, 3569–3578.
64. Islamoglu, F.; Kahveci, B.; Ozil, M.; Akyuz, E.; Mentesh, E.; Ekinici, A.P. Determination of the protonation constants of triazole derivatives in non-aqueous solvents. *Asian J. Chem.* **2009**, *21*, 1453–1459.
65. Ferreira, Q.; Gomes, P.J.; Ribeiro, P.; Jones, N.C.; Hoffmann, S.V.; Mason, N.J.; Oliveira, O.N.; Raposo, M. Determination of Degree of Ionization of Poly(allylamine hydrochloride) (PAH) and Poly[1-[4-(3-carboxy-4 hydroxyphenylazo)benzene sulfonamido]-1,2-ethanediyl, sodium salt] (PAZO) in Layer-by-Layer Films using Vacuum Photoabsorption Spectroscopy. *Langmuir* **2012**, *29*, 448–455. [CrossRef]
66. Zheng, T.; Xu, Z.; Zhao, Y.; Li, H.; Jian, R.; Lu, C. Multiresponsive polysiloxane bearing photochromic spirobenzopyran for sensing pH changes and Fe³⁺ ions and sequential sensing of Ag⁺ and Hg²⁺ ions. *Sensors Actuators B: Chem.* **2018**, *255*, 3305–3315. [CrossRef]
67. Roxburgh, C.J.; Sammes, P.G.; Abdullah, A. Steric and electronically biasing substituent effects on the Photoreversibility of novel, 3'-, 5'- and 3-substituted indolospirobenzopyrans. Thermal evaluation using 1H NMR spectroscopy and Overhauser enhancement studies. *Dye. Pigment.* **2009**, *83*, 31–50. [CrossRef]
68. Brauer, G.M.; Durany, G.; Argentar, H. Ionization Constants of Substituted Benzoic Acids in Ethanol-Water. *J. Res. Natl. Bur. Stand. Sect. A: Phys. Chem.* **1967**, *71*, 379–384. [CrossRef] [PubMed]

69. Sułkowska, A. Interaction of drugs with bovine and human serum albumin. *J. Mol. Struct.* **2002**, *614*, 227–232. [[CrossRef](#)]
70. Lakowicz, J.R. *Principles of fluorescence spectroscopy*; Springer: Berlin/Heidelberg, Germany, 2006.
71. Feng, X.-Z.; Lin, Z.; Yang, L.-J.; Wang, C.; Bai, C. Investigation of the interaction between acridine orange and bovine serum albumin. *Talanta* **1998**, *47*, 1223–1229. [[CrossRef](#)]
72. Scatchard, G. THE ATTRACTIONS OF PROTEINS FOR SMALL MOLECULES AND IONS. *Ann. New York Acad. Sci.* **1949**, *51*, 660–672. [[CrossRef](#)]



© 2020 by the authors. Licensee MDPI, Basel, Switzerland. This article is an open access article distributed under the terms and conditions of the Creative Commons Attribution (CC BY) license (<http://creativecommons.org/licenses/by/4.0/>).